

## Investigation of electronic and elastic properties of $YNi_2-xMx$ (M: Fe, Co, Cu and Zn): Ab initio calculations analyzed with Data mining approach

Mostafa K. Benabadji<sup>1,2\*</sup>, Ammaria Mahmoudi<sup>1</sup>, Djazia Bouabdallah<sup>1</sup>, Fatiha Saidi<sup>1,2</sup>, Houda I. Faraoun<sup>1</sup>, Ghouti Merad<sup>1</sup>

<sup>1</sup> Division Etude et Prédiction des Matériaux (DEPM), Unité de Recherche Matériaux et Energies Renouvelable (URMER), Université Abou Bekr Belkaid, B.P 119 Fg. Pasteur, Tlemcen 13000, Algérie

<sup>2</sup> Ecole Supérieure en Génie Electrique et Energétique (ESGEE), B.P 64, CH2 ACHABA Hanifi, Technopôle USTO 31000 Oran, Algérie

Corresponding Author Email: [kbenabadji@yahoo.fr](mailto:kbenabadji@yahoo.fr)

[https://doi.org/10.18280/ama\\_a.550104](https://doi.org/10.18280/ama_a.550104)

### ABSTRACT

**Received:** 27 March 2018

**Accepted:** 12 April 2018

#### Keywords:

*Ab-initio calculations DFT, laves phases, structural, electronic and elastic properties,  $YNi_2-xMx$  alloys, data mining approach*

We investigated Structural, electronic and mechanical properties of pure  $YNi_2$  and  $YNi_2-xMx$  (M: Fe, Co, Cu and Zn) Laves phases using first principles calculations. Density functional theory is considered within framework of both pseudo-potentials and plane wave's basis using VASP (Vienna ab initio Software Package). The optimized structural parameters were in good agreement with experiment. We calculated formation heat for pure  $YNi_2$  and showed that the cubic C15- $YNi_2$  Laves phase are more stable than C14 and C36 hexagonal phases. We evaluated and discussed Electronic density of states (DOSs) and charge density distribution. The elastic properties were calculated, discussed and analyzed with data mining approach.

## 1. INTRODUCTION

Laves phases are a class of materials presenting an excellent physical and chemical properties [1-10]. These compounds with  $AB_2$  chemical formula, were selected for many large and attractive applications, such as superconducting and hydrogen storage materials, high-temperature and pressure structural materials [11].  $RETM_2$  compounds (RE: Rare Earth, TM: Transition Metals) crystallize for most in the cubic phase C15 type  $MgCu_2$ . Easily absorb hydrogen forming stable hydrides [12]. However, few combinations present some problems regarding their elastic properties such as low hardness and stiffness or high ductility for specific industrial applications. To overcome these issues we can use a partial replacement or alloying with different type of elements.

The  $YNi_2$  compound crystallizes in the C15 structure [13]. A Rare Earth Y ( $d^1s^2$ , space group  $P6_3/mmc$ ,  $a=3.65 \text{ \AA}$ ,  $c=5.73 \text{ \AA}$ ) and a transition metal Ni ( $d^8s^2$ , space group  $Fm\bar{3}m$ ,  $a=3.53 \text{ \AA}$ ) form it. It is a material with industrial requirements making it a good candidate for hydrogen storage. Thus, we were interested to explore these physical properties. Several theoretical works based on first principles calculations, report that Laves phases compounds exhibit a good electronic and mechanical properties such as polar covalent bonding (responsible for the intrinsic stiffness) and a B/G ratio (B : bulk modulus and G : shear modulus) for some compounds close to 1.75, indicating significant ductility and high hardness as well [14-25].

In this paper, we studied the effect of alloying with (M: Fe, Co, Zn and Cu) on  $YNi_2$  properties. Therefore, we used ab initio calculations to examine the structural, elastic and electronic properties of  $YNi_2-xMx$  in  $MgCu_2$  cubic phase for three concentrations ( $x=0.125$ ,  $0.25$  and  $0.375$ ). After relaxation, we obtained optimized lattice parameters and we discussed formation enthalpies, elastic properties and densities

of states.

### 1.2 Computational methods

To determine the physical properties, we performed calculations using the Vienna Ab initio Simulation Package VASP [26-28] code based on the density functional theory (DFT) [29-30]. We used Ultrasoft Vanderbilt type pseudopotentials [31] to describe the interactions between ions and electrons. We applied the generalized gradient approximation GGA (PW91) of Perdew et al. [32] to evaluate the exchange–correlation energies of all examined structures.

We used  $13 \times 13 \times 13$  (cubic C15 structure) and  $13 \times 13 \times 11$  (C14 and C36 structure) sampling of the Brillouin zone generated according to the Monkhorst–Pack scheme [33] and set the cut-off energy (limiting the number of plane waves in the basis) to 320 eV for  $YNi_2$ .

To obtain the equilibrium unit cell volumes, we performed the total energy calculations for each structure with a set of volumes, with all atoms occupying their ideal lattice sites [11]. We fitted curve of total energies versus volumes using murnaghan's equation of state [34].

### 1.2 Data mining techniques

For materials design, not only is the creation of data whether through calculation or experiment important, but a way to analyze the data in a comprehensive and robust manner is also necessary. Some of the challenges in searching through discrete data include the difficulty of analyzing large amounts of data, understanding the correlations among various properties, and using the correlations to better understand the underlying physics of the system. Utilizing a multivariate analysis, the data can be examined so that trends and correlations become apparent.

Data mining is employed in this work in order to fully uncover inter-correlations in the data. Additionally, the mathematical relationship between descriptors must be developed before descriptor reduction is possible. Once the relationships are known then the model can be accurately extended to new data so that a virtual system can be fully described with limited data. The data mining method used here is principal component analysis (PCA) [35], which is a powerful statistical approach for the analysis of materials properties and has been used to address a variety of physics and materials science issues [36-37].

PCA is a classification method, which projects the spatial data into a set of principal components (PC) and maps the data on a dimensionally reduced space. The PC capturing the most information is associated with the eigenvalue corresponding with the largest eigenvalue of the covariance matrix of the original dataset. All PC's are orthogonal to each other, and thus each captures unique information. The advantage of PCA is that typically, a few PC's are sufficient for describing a system, and a dataset of n-dimensions can be reduced to a few dimensions with minimal loss of information [38]. The PC's do not necessarily have an obvious physical meaning, but rather are a combination of variables, which explain the largest variation in the data. The reduction in dimensionality makes trends and correlations, which are "hidden" in the data to become easily visualized and described in PC space. PCA decomposes the original data matrix into the scores and loadings matrices, where the scores values classify the samples and the loadings values classify the descriptors in terms of their separation of the samples. The correlations among the descriptors become obvious in a PCA analysis, and by defining the correlations in the data, we can then reduce the number of descriptors to a minimum to permit a more convenient data analysis.

## 2. RESULTS AND DISCUSSIONS

### 2.1 Structural stability of pure YNi<sub>2</sub>

These calculations allowed us to determine the most stable structure among hexagonals (C14 and C36) and cubic C15 Laves phases.

**Table 1.** Equilibrium values of the three units cells: the lattice constants (a, b, c in Å) and bulk modulus (GPa) for both phases calculated with GGA, compared with other values listed in parentheses

|                                    | a (Å)       | b (Å) | c (Å) | B <sub>0</sub> | B' <sub>0</sub> |
|------------------------------------|-------------|-------|-------|----------------|-----------------|
| C14                                | 5.08        | -     | 8.34  | 117.3          | 4.26            |
| Space group : P6 <sub>3</sub> /mmc |             |       |       | 0              | 8               |
| C36                                | 5.08        | -     | 16.67 | 118.3          | 4.09            |
| Space group: P6 <sub>3</sub> /mmc  |             |       |       | 9              | 8               |
| C15                                | 7.18        | -     | -     | 119.2          | 4.55            |
| Space group: Fd3m                  | (7.22)<br>a | -     | -     | 0              | 3               |

<sup>a</sup>Ref. [13]

We obtained the cell parameters and bulk modulus (Table 1) for C14, C15 and C36 Laves phases after fitting the curve of total energy versus volume (Figure1).

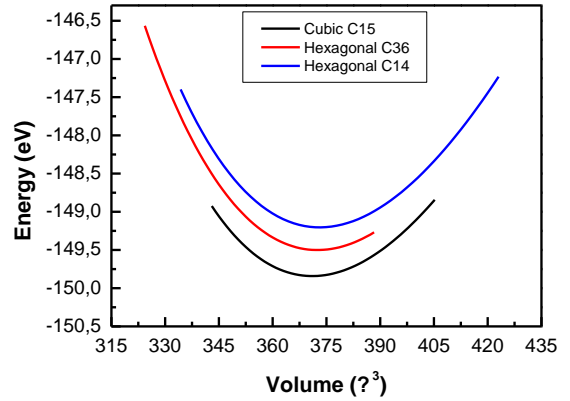


**Figure 1.** Total energy versus volume for YNi<sub>2</sub> compound crystallized in C14, C15 and C36 Laves phases

In Figure 1, we noticed that the equilibrium volumes of the three studied phases were almost equal indicating a possibility of observing a phase transition according to the temperature. We found that the cubic C15 phase is the most stable structure.

### 2.2 Formation enthalpies and volume

In order to investigate the alloying ability and stability, we calculated the formation energy ( $\Delta E_f$ ) of AB<sub>2</sub> type Laves phase by [15]:

$$\Delta E_f = E_{\text{tot}}^{\text{AB}_2} - (E_{\text{solid}}^{\text{A}} + 2E_{\text{solid}}^{\text{B}}) \quad (1)$$

We calculated the formation energy ( $\Delta E_f^{\text{alloy}}$ ) of AB<sub>2-x</sub>C<sub>x</sub> alloy by [39]:

$$\Delta E_f^{\text{alloy}} = E_{\text{tot}}^{\text{AB}_{2-x}\text{C}_x} - (E_{\text{solid}}^{\text{A}} + (2-x)E_{\text{solid}}^{\text{B}} + xE_{\text{solid}}^{\text{C}}) \quad (2)$$

**Table 2.** Equilibrium volume and heats of formation of the YNi<sub>2</sub> intermetallic compound and their alloys (per formula unit, other value given in parentheses)

| Compounds                                |  | Volume (Å <sup>3</sup> /f.u.) | Enthalpies $\Delta H_{\text{form}}$ (eV/f.u.) |
|--|--|-------------------------------|---|
| C14                                      | YNi <sub>2</sub>                         | 46.59                         | -1.405  |
| C36                                      | YNi <sub>2</sub>                         | 46.56                         | -1.442  |
| C15                                      | YNi <sub>2</sub>                         | 46.26                         | -1.476  |
|  |  | (47.18) <sup>a</sup>          | (-1.45) <sup>a</sup>                          |
|  |  | (45.90) <sup>b</sup>          | (-1.21) <sup>c</sup>                          |
| C15                                      | YNi <sub>1.875</sub> Zn <sub>0.125</sub> | 46.99                         | -1.442  |
|  | YNi <sub>1.75</sub> Zn <sub>0.25</sub>   | 47.68                         | +1.103  |
|  | YNi <sub>1.875</sub> Cu <sub>0.125</sub> | 46.64                         | -1.438  |
|  | YNi <sub>1.75</sub> Cu <sub>0.25</sub>   | 46.95                         | -1.376  |
|  | YNi <sub>1.625</sub> Cu <sub>0.375</sub> | 47.12                         | +1.010  |
|  | YNi <sub>1.875</sub> Co <sub>0.125</sub> | 46.28                         | -1.454  |
|  | YNi <sub>1.75</sub> Co <sub>0.25</sub>   | 46.21                         | -1.415  |
|  | YNi <sub>1.625</sub> Co <sub>0.375</sub> | 46.10                         | -1.376  |
|  | YNi <sub>1.875</sub> Fe <sub>0.125</sub> | 46.34                         | -1.419  |
|  | YNi <sub>1.75</sub> Fe <sub>0.25</sub>   | 46.28                         | -1.358  |
| YNi <sub>1.625</sub> Fe <sub>0.375</sub> | 46.19                                    | -1.299                        |   |

<sup>a</sup>Ref. [13]

<sup>b</sup>Ref. [36]

<sup>c</sup>Ref. [37]

$E_{\text{solid}}^A$ ,  $E_{\text{solid}}^B$  and  $E_{\text{solid}}^C$  represent the energy per atom of A, B and C in solid states.

At zero Kelvin and under pressure zero Pa, the enthalpy equals to the energy, that is  $\Delta E_f(\text{AB}_2) = \Delta H_f(\text{AB}_2)$  and  $\Delta E_f^{\text{alloy}} = \Delta H_f^{\text{alloy}}$  [40].

From table 2, we can see that the heats of formation for  $\text{YNi}_2$  are -1.405, -1.442 and -1.476 eV/atom for C14, C36 and C15 structures, respectively. These values showed that the lowest heat of formation for  $\text{YNi}_2$  correspond to the C15 structure Laves phase. Relaxed systems with different transition metals (Fe, Co, Cu and Zn) studied for three concentrations 0.125, 0.25 and 0.375 showed negative  $\Delta H_{\text{form}}$  values except for  $\text{YNi}_{1.75}\text{Zn}_{0.25}$  and  $\text{YNi}_{1.625}\text{Cu}_{0.375}$  (+1.103 and +1.010 eV/atom respectively). They crystallized in cubic C15 structure with a little volume distortion compared to the pure system. Concentration of Zn or Cu atoms above 0.25 in  $\text{YNi}_2$ -C15 matrix imply an important deformation. So the loss of the structural symmetry.

## 2.3 Elastic properties

The elastic properties can give valuable information about the nature of binding between neighboring atomic planes. Usually, the  $C_{ij}$  elastic constants can define significantly the anisotropic binding characteristics and structural stability. These constants have been frequently associated to the shear modulus G and Young's modulus E. Ab initio calculations of these constants requires accurate methods. A popular approach is used to evaluate the elastic constants from their known structure [16, 41-45].

The afore mentioned intermetallic compounds have very appealing mechanical properties. To show that, we were interested to calculate the elastic constants for  $\text{YNi}_2$  and their alloys for C15 structure type Laves phase.

The three independent elastic constants  $C_{11}$ ,  $C_{12}$  and  $C_{44}$  characterize the cubic C15 structure. The obtained values for studied systems are presented in Table 3. We report that the elastic constants of these compounds are not determined experimentally.

**Table 3.** The calculated elastic constants, bulk modulus B (GPa), shear modulus G (GPa), Young's modulus E (GPa), Poisson's ratio  $\nu$ , ratio B/G, Cauchy pressure  $C_{12}$ - $C_{44}$  and Anisotropy factor A

| Compounds                             | $C_{11}$ | $C_{12}$ | $C_{44}$ | B      | G     | E      | $\nu$ | B/G  | $C_{12}$ - $C_{44}$ | A     |
|---------------------------------------|----------|----------|----------|--------|-------|--------|-------|------|---------------------|-------|
| $\text{YNi}_2$                        | 164.15   | 96.72    | 34.14    | 119.20 | 33.97 | 93.07  | 0.370 | 3.51 | 62.58               | 1.012 |
| $\text{YNi}_{1.875}\text{Zn}_{0.125}$ | 225.01   | 57.31    | 86.28    | 113.21 | 85.30 | 204.53 | 0.190 | 1.33 | -28.97              | 1.028 |
| $\text{YNi}_{1.875}\text{Cu}_{0.125}$ | 221.87   | 61.59    | 81.61    | 115.02 | 81.02 | 196.83 | 0.210 | 1.42 | -20.02              | 1.018 |
| $\text{YNi}_{1.75}\text{Cu}_{0.25}$   | 221.86   | 58.08    | 84.87    | 112.67 | 83.66 | 201.20 | 0.200 | 1.35 | -26.79              | 1.036 |
| $\text{YNi}_{1.875}\text{Co}_{0.125}$ | 221.39   | 66.59    | 78.95    | 118.19 | 78.33 | 192.46 | 0.228 | 1.51 | -12.36              | 1.020 |
| $\text{YNi}_{1.75}\text{Co}_{0.25}$   | 221.58   | 69.44    | 77.19    | 120.15 | 76.74 | 189.81 | 0.236 | 1.57 | -7.75               | 1.015 |
| $\text{YNi}_{1.625}\text{Co}_{0.325}$ | 222.416  | 68.25    | 80.16    | 119.64 | 78.91 | 194.06 | 0.230 | 1.52 | -11.91              | 1.036 |
| $\text{YNi}_{1.875}\text{Fe}_{0.125}$ | 220.03   | 66.91    | 79.73    | 118.06 | 78.44 | 192.67 | 0.228 | 1.51 | -12.82              | 1.041 |
| $\text{YNi}_{1.75}\text{Fe}_{0.25}$   | 209.87   | 75.55    | 57.58    | 120.32 | 61.24 | 157.06 | 0.282 | 1.96 | 17.96               | 0.857 |
| $\text{YNi}_{1.625}\text{Fe}_{0.375}$ | 218.59   | 72.74    | 68.35    | 121.36 | 70.15 | 176.44 | 0.258 | 1.73 | 4.39                | 0.940 |

For the C15 cubic phase, the independent single-crystal elastic constants ( $C_{11}$  and  $C_{12}$ ) can be derived from the bulk modulus B and tetragonal shear modulus C' defined by the following equations  $B = (C_{11} + 2C_{12}) / 3$  and  $C' = (C_{11} - C_{12}) / 2$ . The  $C_{44}$  constant is the trigonal shear modulus. We calculated these constants using the scheme described in detail by Mehl et al. [42]. Polycrystalline elastic modulus is obtainable by taking the average of single elastic constants in several schemes. Both Voigt  $G_V$  [46] and Reuss  $G_R$  [47] components of shear modulus are the upper and lower theoretical limits of the real shear modulus, respectively. They are described as [48]:

$$G_V = \frac{C_{11} - C_{12} + 3C_{44}}{5} \quad (3)$$

$$G_R = \frac{5(C_{11} - C_{12})C_{44}}{3(C_{11} - C_{12}) + 4C_{44}} \quad (4)$$

The real shear modulus G and the Young's modulus E can be written respectively as:

$$G = \frac{1}{2}(G_V + G_R) \quad (5)$$

$$E = \frac{9BG}{3B+G} \quad (6)$$

The Poisson's ratio  $\nu$  and elastic anisotropy A are obtained by the following expressions:

$$\nu = \frac{3B-2G}{2(3B+G)} \quad (7)$$

$$A = 2 \frac{C_{44}}{C_{11} - C_{12}} \quad (8)$$

The bulk B, shear G and Young's E modulus, Poisson's  $\nu$  and B/G coefficients and anisotropy factor A for the three compounds are listed in Table 3.

The ductility of the material is indicated by the B/G ratio. If  $B/G \geq 1.75$ , the compound should have important ductility. For pure C15- $\text{YNi}_2$  compound and  $\text{YNi}_{2-x}\text{M}_x$  systems ( $x=0.125, 0.25$  and  $0.375$ ),  $A \approx 1$  indicating isotropic elasticity except for  $\text{YNi}_{1.75}\text{Fe}_{0.25}$  where  $A=0.857$ .

In general, If the Poisson's ratio  $\nu$ :  $-1 \leq \nu \leq 0.5$ , the polar covalent bonding is determined. If  $\nu \approx 1/3$ , the compound is ductile. If  $\nu < 1/3$  the material becomes brittle.

As seen in Table 3, the pure  $\text{YNi}_2$  has a B/G ratio equal to 3.51 indicating a high ductility due high compression modulus

B and low shear modulus G. This latter is confirmed by Poisson's ratio with a value of  $0.37 \approx 1/3$ . Whereas, for all alloys, the mechanical behavior is changed by M-atoms addition, so the B/G ratio took values between 1.33 and 1.57, due to the high value of shear modulus G with a slight change in the value of the bulk modulus B, except for  $\text{YNi}_{1.75}\text{Fe}_{0.25}$  and  $\text{YNi}_{1.625}\text{Fe}_{0.375}$  (1.93 and 1.73 respectively). Otherwise, The Young's modulus E has a very high values compared to the pure  $\text{YNi}_2$ , revealing a decreasing in ductility and increasing in stiffness for the some alloys. Moreover, the Poisson's ratio decreased under  $1/3$ .

## 2.4 Electronic properties

Structural stability and mechanical properties of  $\text{YNi}_2$  and its alloys  $\text{YNi}_{2-x}\text{Zn}_x$  are related to their chemical bonding nature so it was necessary to perform electronic densities of state (DOS) calculation.

## 2.5 Pure $\text{YNi}_2$

Total and partial DOS and electron charge densities distribution of pure  $\text{YNi}_2$  are presented in Figs. 2 and 3, respectively.

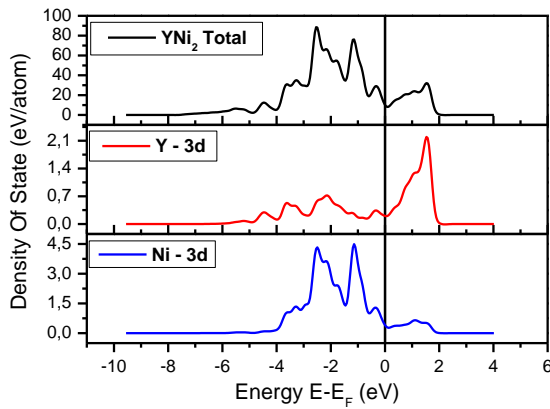


**Figure 2.** Total and partial density of state of pure  $\text{YNi}_2$

As shown in Fig. 2, before Fermi level and between -4 to 0 eV, the total DOS is dominated by Ni d states. The metallic character is due to the presence of electronic states of Ni atoms. The effect of Y atoms is considered negligible compared to that of Ni atoms at Fermi level.

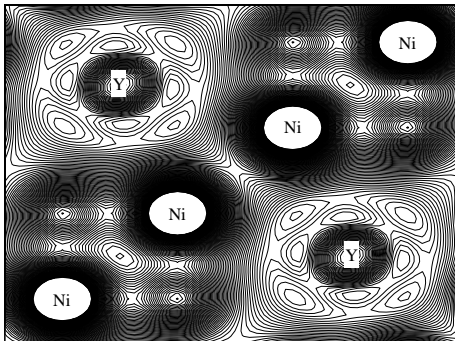


**Figure 3.** The contour plots of charge densities. The (010) plan for cubic-C15 structure of pure  $\text{YNi}_2$

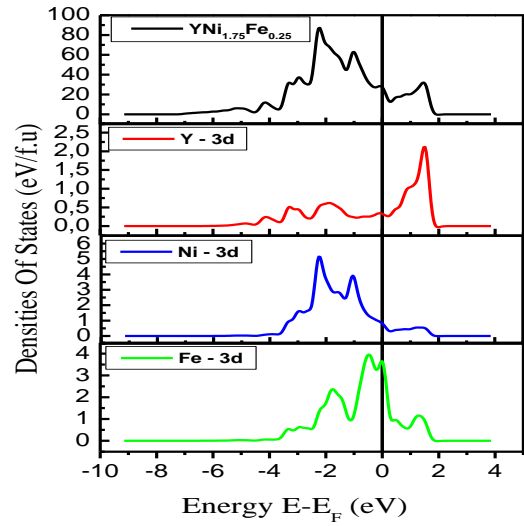


**Figure 4.** Calculated total and partial DOS of  $\text{YNi}_{1.75}\text{Fe}_{0.25}$  compound

In Fig.3, we displayed the contour maps of the electron densities in the (010) plane for C15- $\text{YNi}_2$  phase.

To determine the nature of existing chemical bonds, it was interesting to plot the electronic charges density contours of C15- $\text{YNi}_2$  compound (Fig.3). We noticed that the distribution of charges is maximum between the Ni atoms, confirming the strong metallic character, validating what was observed earlier in the  $\text{YNi}_2$  DOS (Fig.2).

The  $\text{YNi}_{2-x}\text{Fe}_x$  alloys:

Electronic densities of state of  $\text{YNi}_{1.875}\text{Fe}_{0.25}$  and  $\text{YNi}_{1.625}\text{Fe}_{0.375}$  alloys are presented in Figs. 4 and 5. Where some effects of incorporated Fe atoms in pure compound are discussed.

As seen in Fig.4 and Fig.5 the effect of Fe atom in the  $\text{YNi}_2$ -DOS. Fermi level was shifted towards the negative values. This displacement is accompanied by increase in the metallic character compared to the pure system.

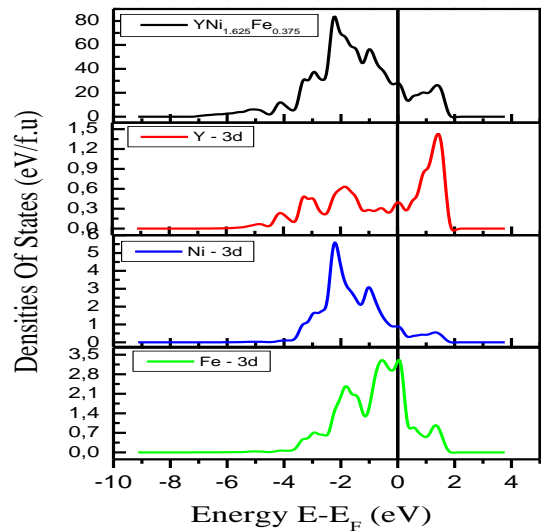


**Figure 5.** Calculated total and partial DOS of  $\text{YNi}_{1.625}\text{Fe}_{0.375}$  compound

The Fe-3d states are localized and form two peaks between -2 eV and 0 eV. They strengthened the polar covalency in the

Ni-3d-Fe-3d bonds for both alloys compared to pure YNi<sub>2</sub>, which explain the Young modulus E increase (Table 3). So the previous analysis of the elastic properties are validated.

## 2.6 Data mining results

In order to identify the trends or clustering in materials property data, we construct a database for several intermetallic YNi<sub>2-x</sub>M<sub>x</sub> [(M: Fe, Co, Cu and Zn), (x:0, 0.125, 0.25 and 0.375)] including the, elastic constants, bulk and shear modulus, young modulus, Poisson's ratio  $\nu$ , the B/G ratio, the Cauchy pressure and Anisotropy ratio A. Table 3 contains a portion of the dataset used.

The first analysis done was to examine the general trends in different intermetallics. The resulting score plot of this analysis is shown in Fig.6.

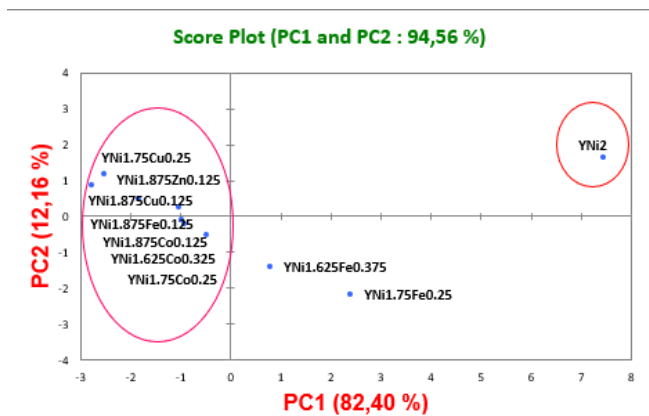


**Figure 6.** PCA and PLS score plot of different polar intermetallics

For this analysis, the sign of each principal component has only relational meaning. PC1 captures 82.40% of the variance in the dataset, and PC2 captures 12.16% of the variance as seen in fig.6. No other PCs are included in any of the discussions because they do not provide significant information.

From looking at this figure it appears three important clustering those with positive PC1 which we will refer to cluster 1 [YNi<sub>2</sub>] and cluster 2 [YNi<sub>1.625</sub>Fe<sub>0.375</sub>, YNi<sub>1.75</sub>Fe<sub>0.25</sub>], and those with a negative PC1 which we will refer to cluster3 [YNi<sub>1.875</sub>Zn<sub>0.125</sub>, YNi<sub>1.875</sub>Cu<sub>0.125</sub>, YNi<sub>1.75</sub>Cu<sub>0.25</sub>, YNi<sub>1.875</sub>Co<sub>0.125</sub>, YNi<sub>1.75</sub>Co<sub>0.25</sub>, YNi<sub>1.625</sub>Co<sub>0.325</sub>, YNi<sub>1.875</sub>Fe<sub>0.125</sub>].

In a first insight it appears that cluster 1 and 2 includes intermetallics with high B/G ratio, high Cauchy pressure C12-C44, high bulk modulus (B), and low shear modulus G, while cluster 3 is characterized by low B/G ratio, and high G and E.

Compounds of first cluster1 is highly correlated with B/G ratio and the Cauchy pressure (C12-C44) indicating the ductility of this material.

However, Materials of the second cluster are highly correlated with bulk modulus B and B/G ratio indicating that these materials are hard with appreciable ductility, this result confirms that the addition of simple concentration of Fe can decrease ductility of YNi<sub>2</sub> and increase its hardness, which is in consistent with ab initio observations.

Materials of cluster 3 are highly correlated with shear modulus G and the young modulus E indicating the rigidity of these materials.

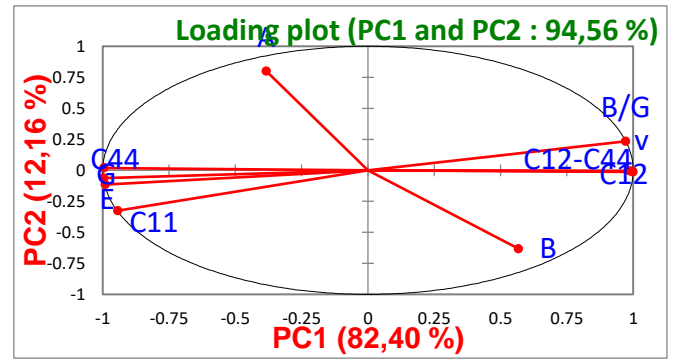


**Figure 7.** PCA and PLS loading plot of different elastic parameters

The loading plot corresponds with the score plot but represents the variance among descriptors. Fig.7 shows the loading plot corresponding with the samples shown in Fig. 6.

The axes of the score plot and loading plot are the same so the information in the plots can be compared directly.

According to the Fig. 6 and 7 we notice that the position of the properties G and B/G are correlated to cluster3 and cluster1 respectively. Properties with similar PC values are highly correlated, while inverse PC values indicate inverse correlations. Therefore, the properties in cluster 1 and 2 are inversely correlated with the properties in cluster 3, while the properties within clusters 2 are highly correlated with other properties within the same cluster. Many of the correlations between properties are not obvious. One correlation that is expected is the connection between the G and B/G, that means that if the hardness increases the ductility decreases which is consistent with the experimental observations and our ab initio calculations. Whereas G, C44 and E they all have a negative PC2 and PC1 values, so they are highly correlated and indicate hardness of materials of cluster 3. The ratio B/G and Cauchy pressure (C12-C44) are highly correlated, which is consistent with the fact that materials with high B/G and (C12-C44) are highly ductile.

The relationship of all intermetallics and corresponding parameters is clearly shown in the biplot of Fig.8 according to the data listed in Table 3.

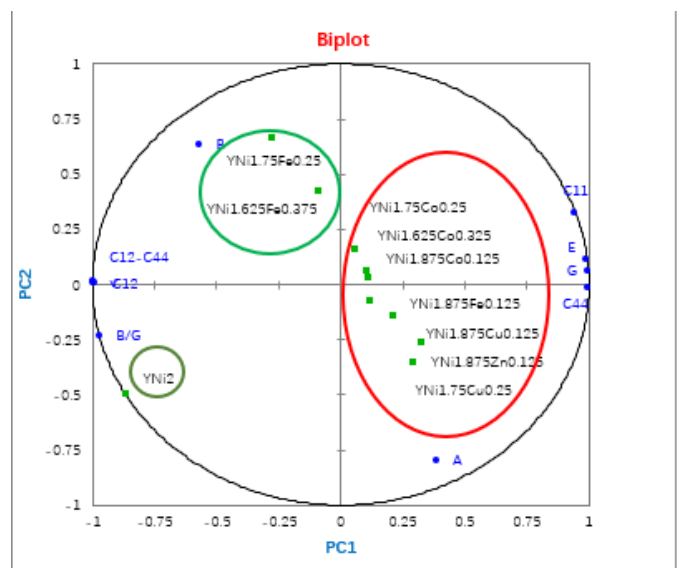


**Figure 8.** The biplot of different polar intermetallics and elastic parameters

This biplot obtained by PCA combines properties and criterions with different intermetallics. For this analysis, the sign of each principal component has only relative meaning. From looking at these figures it appears that materials of the first cluster are correlated with indicators of the ductility (B/G, C12–C44), those of the third cluster are highly correlated with the rigidity (E,G) indicators ,however , the compounds of the second cluster are highly correlated with hardness criterions (B) which validate our ab-initio results.

### 3. CONCLUSION

In this work, we analyzed the structural properties for  $\text{YNi}_2$  compound, and we observe that  $\text{YNi}_2$  crystallized in the cubic C15 structure. Heats of formation of  $\text{YNi}_{2-x}\text{M}_x$  carried out that only  $\text{YNi}_{1.75}\text{Zn}_{0.25}$  and  $\text{YNi}_{1.625}\text{Cu}_{0.375}$  present positive values.

To complete the fundamental characteristics of these compounds we have analyzed their mechanical properties. A critical analysis has been carried out using data mining techniques. The major goal was to predict the better hard materials with appreciable ductility. The present results clearly demonstrate that a simple visual observation of the PCA plots, in respect to the position of different intermetallics concludes that  $\text{YNi}_{1.625}\text{Fe}_{0.375}$ ,  $\text{YNi}_{1.75}\text{Fe}_{0.25}$  intermetallics have good hardness and appreciable ductility compared to  $\text{YNi}_{1.875}\text{Zn}_{0.125}$ ,  $\text{YNi}_{1.875}\text{Cu}_{0.125}$ ,  $\text{YNi}_{1.75}\text{Cu}_{0.25}$ ,  $\text{YNi}_{1.875}\text{Co}_{0.125}$ ,  $\text{YNi}_{1.75}\text{Co}_{0.25}$ ,  $\text{YNi}_{1.625}\text{Co}_{0.325}$  and  $\text{YNi}_{1.875}\text{Fe}_{0.125}$  compounds which present good rigidity. However, our results confirm that these intermetallics present very interesting mechanical properties. It was found that the  $\text{YNi}_2$  is the most ductile, while  $\text{YNi}_{1.875}\text{Zn}_{0.125}$  the most rigid structure of these series of compounds. We can explain this result that the addition of simple concentration of Fe can decrease ductility of  $\text{YNi}_2$  and increase its hardness, which is in consistent with ab initio observations. Finally, our results reveal that Fe based systems are the most interesting by their high rigidity and appreciable ductility.

### REFERENCES

- [1] Ross JW, Crangle J. (1964). Magnetization of cubic laves phase compounds of rare earths with cobalt, Physical Review 133: A509-A510. <https://doi.org/10.1103/PhysRev.133.A509>
- [2] McDermott MJ, Marklund KK. (1969). Partial quenching of rare earth moment in cubic laves intermetallic compounds, Journal of Applied Physics 40: 1007-1008. <https://doi.org/10.1063/1.1657505>
- [3] Ormeci A, Chu F, Wills JM, Mitchell TE, Albers RC, Thoma DJ, Chen SP. (1996). Total-energy study of electronic structure and mechanical behavior of C15 Laves phase compounds:  $\text{NbCr}_2$  and  $\text{HfV}_2$ . Physical Review B 54: 12753-12762. <https://doi.org/10.1103/PhysRevB.54.12753>
- [4] Roth J. (2005). Shock waves in complex binary solids: Cubic Laves crystals, quasicrystals, and amorphous solids, Physical Review B 71: 064102. <https://doi.org/10.1103/PhysRevB.71.064102>
- [5] Liu JJ, Ren WJ, Zhang ZD, Li D, Li J, Zhao XG, Liu W, Or SW. (2006). Spin configuration and magnetostrictive properties of Laves compounds  $\text{Tb}_x\text{Dy}_{0.7-x}\text{Pr}_{0.3}$  ( $\text{Fe}_{0.9}\text{B}_{0.1}$ ) $_{1.93}$  ( $0.10 \leq x \leq 0.28$ ). Journal of Applied Physics: 100 023904. <https://doi.org/10.1063/1.2219344>
- [6] Wu Z, Saini NL, Agrestini S, Castro DD, Bianconi A, Marcelli A, Battisti M, Gozzi D, Balducci G. (2000). Ru K-edge absorption study on the  $\text{La}_{1-x}\text{Ce}_x\text{Ru}_2$  system. Journal of Physics: Condensed Matter 12: 6971. <https://doi.org/10.1088/0953-8984/12/30/324>
- [7] Nagasako N, Fukumoto A, Miwa K. (2002). First-principles calculations of C14-type Laves phase Ti-Mn hydrides. Physical Review B 66: 155106. <https://doi.org/10.1103/PhysRevB.66.155106>
- [8] Hong S, Fu CL. (2002). Hydrogen in Laves phase  $\text{ZrX}_2$  ( $X=\text{V, Cr, Mn, Fe, Co, Ni}$ ) compounds: Binding energies and electronic and magnetic structure. Physical Review B 66: 094109. <https://doi.org/10.1103/PhysRevB.66.094109>
- [9] Uchida H, Matsumura Y, Uchida H, Kaneko H. (2002). Progress in thin films of giant magnetostrictive alloys. Journal of Magnetism and Magnetic Materials 239: 540-545. [https://doi.org/10.1016/s0304-8853\(01\)00659-x](https://doi.org/10.1016/s0304-8853(01)00659-x)
- [10] Liu CT, Zhu JH, Brady MP, McKamey CG, Pike LM. (2000). Physical metallurgy and mechanical properties of transition-metal laves phase alloys, Intermetallics 8: 1119-1129. [https://doi.org/10.1016/s0966-9795\(00\)00109-6](https://doi.org/10.1016/s0966-9795(00)00109-6)
- [11] Tao X, Ouyang Y, Liu H, Zeng F, Feng Y, Du Y, Jin Z. (2008). Ab initio calculation of the total energy and elastic properties of laves phase c15  $\text{Al}_2\text{Re}$  ( $\text{Re} = \text{Sc, Y, La, Ce-Lu}$ ). Computational Materials Science: 44 392-399. <https://doi.org/10.1016/j.commatsci.2008.03.036>
- [12] Srinivas G, Sankaranarayanan V, Ramaprabhu S. (2008). Thermodynamic and kinetic properties of  $\text{Ho}_{1-x}\text{Ti}_x\text{Co}_2$ -hydrogen system. Journal of Physics and Chemistry of Solids 69: 1869-1876. <https://doi.org/10.1016/j.jpics.2007.11.016>
- [13] Lindbaum A, Hafner J, Gratz E, Heathman S. (1998). Diffraction, structural stability of  $\text{YM}_2$  compounds ( $M = \text{Al, Ni, Cu}$ ) studied by *ab initio* total-energy calculations and high-pressure X-ray diffraction. Journal of Physics: Condensed Matter 10: 2933. <https://doi.org/10.1088/0953-8984/10/13/011>
- [14] Sari A, Merad G, Abdelkader HS. (2015). Ab initio calculations of structural, elastic and thermal properties of  $\text{TiCr}_2$  and  $(\text{Ti,Mg})(\text{Mg,Cr})_2$  Laves phases. Computational Materials Science 96 part a: 348-353. <https://doi.org/10.1016/j.commatsci.2014.09.040>
- [15] Benabadji MK, Faraoun HI, Abdelkader HS, Dergal M, Hlil EK, Merad G. (2013). Structural stability and electronic structure study of  $\text{YCu}_2$ - $\text{YZn}_2$  laves phases by first-principles calculations. Computational Materials Science 77: 366-371. <https://doi.org/10.1016/j.commatsci.2013.04.067>
- [16] Saidi F, Benabadji MK, Faraoun HI, Aourag H. (2014). Structural and mechanical properties of laves phases  $\text{YCu}_2$  and  $\text{YZn}_2$ : First principles calculation analyzed with data mining approach. Computational Materials Science 89: 176-181. <https://doi.org/10.1016/j.commatsci.2014.03.053>
- [17] Chen S, Sun Y, Duan YH, Huang B, Peng MJ. (2015). Phase stability, structural and elastic properties of C15-type Laves transition-metal compounds  $\text{MCo}_2$  from first-principles calculations. Journal of Alloys and

- Compounds 630: 202-208.  
<https://doi.org/10.1016/j.jallcom.2015.01.038>
- [18] Hu WC, Liu Y, Li DJ, Zeng XQ, Xu CS. (2014). First-principles study of structural and electronic properties of c14-type Laves phase  $Al_2Zr$  and  $Al_2Hf$ . *Computational Materials Science* 83: 27-34. <https://doi.org/10.1016/j.commatsci.2013.10.029>
- [19] Mao P, Yu B, Liu Z, Wang F, Ju Y. (2014). Mechanical, electronic and thermodynamic properties of  $Mg_2Ca$  laves phase under high pressure: A first-principles calculation, *Computational Materials Science* 88: 61-70. <https://doi.org/10.1016/j.commatsci.2014.03.006>
- [20] Liu Y, Hu WC, Li DJ, Li K, Jin HL, Xu YX, Xu CS, Zeng XQ. (2015). Mechanical, electronic and thermodynamic properties of C14-type  $AMg_2$  (A = Ca, Sr and Ba) compounds from first principles calculations. *Computational Materials Science* 97: 75-85. <https://doi.org/10.1016/j.commatsci.2014.10.005>
- [21] Connétable D, Mathon M, Lacaze J. (2011). First principle energies of binary and ternary phases of the Fe–Nb–Ni–Cr system. *Calphad*, 35: 588-593. <http://dx.doi.org/10.1016/j.calphad.2011.09.004>
- [22] Anton H, Schmidt PC. (1997). Theoretical investigations of the elastic constants in Laves phases. *Intermetallics* 5: 449-465. [https://doi.org/10.1016/s0966-9795\(97\)00017-4](https://doi.org/10.1016/s0966-9795(97)00017-4)
- [23] Nong ZS, Zhu JC, Cao Y, Yang XW, Lai ZH, Liu Y. (2013). A first-principles study on the structural, elastic and electronic properties of the C14 Laves phase compounds  $tix_2$  (X=Cr, Mn, Fe). *Physica B: Condensed Matter* 419: 11-18. <https://doi.org/10.1016/j.physb.2013.03.012>
- [24] Yu W, Wang N, Xiao X, Tang B, Peng L, Ding W. (2009). First-principles investigation of the binary  $AB_2$  type Laves phase in Mg–Al–Ca alloy: Electronic structure and elastic properties. *Solid State Sciences*: 111400. <https://doi.org/10.1016/j.solidstatesciences.2009.04.017>
- [25] Chen XQ, Wolf W, Podloucky R, Rogl P. (2005). Ab initio study of ground-state properties of the Laves phase compounds  $TiCr_2$ ,  $ZrCr_2$ , and  $HfCr_2$ , *Physical Review B* 71: 174101. <https://doi.org/10.1103/PhysRevB.71.174101>
- [26] Kresse G, Furthmüller J. (1996). Efficient iterative schemes for *ab initio* total-energy calculations using a plane-wave basis set. *Physical Review B* 54: 11169-11186. <https://doi.org/10.1103/PhysRevB.54.11169>
- [27] Kresse G, Furthmüller J. (1996). Efficiency of ab-initio total energy calculations for metals and semiconductors using a plane-wave basis set. *Computational Materials Science* 6: 15-50. [https://doi.org/10.1016/0927-0256\(96\)00008-0](https://doi.org/10.1016/0927-0256(96)00008-0)
- [28] Kresse G, Joubert D. (1999). From ultrasoft pseudopotentials to the projector augmented-wave method. *Physical Review B* 59: 1758-1775. <https://doi.org/10.1103/PhysRevB.59.1758>
- [29] Hohenberg P, Kohn W. (1964). Inhomogeneous electron gas. *Physical Review*: 136 B864-B871. <https://doi.org/10.1103/PhysRev.136.B864>
- [30] Kohn W, Sham LJ. (1965). Self-consistent equations including exchange and correlation effects, *Physical Review* 140: A1133-A1138. <https://doi.org/10.1103/PhysRev.140.A1133>
- [31] Vanderbilt D. (1990). Soft self-consistent pseudopotentials in a generalized eigenvalue formalism. *Physical Review B* 41: 7892-7895. <https://doi.org/10.1103/PhysRevB.41.7892>
- [32] Perdew JP, Chevary JA, Vosko SH, Jackson KA, Pederson MR, Singh DJ, Fiolhais C. (1992). Atoms, molecules, solids, and surfaces: Applications of the generalized gradient approximation for exchange and correlation, *Physical Review B*, 466671-6687. <https://doi.org/10.1103/PhysRevB.46.6671>
- [33] Monkhorst HJ, Pack JD. (1976). Special points for Brillouin-zone integrations, *Physical Review B* 13: 5188-5192. <https://doi.org/10.1103/PhysRevB.13.5188>
- [34] Tyuterev VG, Vast N. (2006). Murnaghan's equation of state for the electronic ground state energy. *Computational Materials Science* 38: 350-353. <https://doi.org/10.1016/j.commatsci.2005.08.012>
- [35] Suh C, Rajan K. (2005). Virtual screening and QSAR formulations for crystal chemistry. *QSAR & Combinatorial Science* 24: 114. <https://doi.org/10.1002/qsar.200420057>
- [36] Suh CKR, Vogel BM, Narasimhan B, Mallapragada SK. (2007). *Combinatorial materials science*, edited by Mallapragada SK, Narasimhan B, and Porter MD (John Wiley-Interscience, Hoboken, NJ).
- [37] Broderick S, Rajan K. (2011). *Proceedings of the first World Congress on Integrated Computational Materials*, TMS, Wiley,
- [38] Ericksson L, Johansson E, Kettaneh-wold N, Wold S, Umetrics AB. 2001. Umea.
- [39] Zhang RJ, Wang YM, Lu MQ, Xu DS, Yang K. (2005). First-principles study on the crystal, electronic structure and stability of  $LaNi_{5-x}Al_x$  (x = 0, 0.25, 0.5, 0.75 and 1). *Acta Materialia* 53: 3445-3452. <https://doi.org/10.1016/j.actamat.2005.04.005>
- [40] Fang CM, Huis MAV, Zandbergen HW. (2012). Stability and structures of the CFCC-TmC phases: A first-principles study. *Computational Materials Science* 51: 146-150. <https://doi.org/10.1016/j.commatsci.2011.07.017>
- [41] Gratz E, Lindbaum A. (1994). The influence of the magnetic state on the thermal expansion in 1:2 rare earth intermetallic compounds. *Journal of Magnetism and Magnetic Materials* 137: 115-121. [https://doi.org/10.1016/0304-8853\(94\)90195-3](https://doi.org/10.1016/0304-8853(94)90195-3)
- [42] Colinet C, Pasturel A, Buschow KHJ. (1987). Short-range order and stability in Gd-Ni and Y-Ni systems. *Journal of Applied Physics*: 623712-3717. <https://doi.org/10.1063/1.339253>
- [43] Mehl MJ. (1993). Pressure dependence of the elastic moduli in aluminum-rich Al-Li compounds. *Physical Review B* 47: 2493-2500. <https://doi.org/10.1103/PhysRevB.47.2493>
- [44] Khenata R, Bouhemadou A, Reshak AH, Ahmed R, Bouhafs B, Rached D, Al-Douri Y, Rérat M. (2007). First-principles calculations of the elastic, electronic, and optical properties of the filled skutterudites  $CeFe_4P_{12}$  and  $ThFe_4P_{12}$ . *Physical Review B* 75: 195131. <https://doi.org/10.1103/PhysRevB.75.195131>
- [45] Bouhemadou A, Khenata R, Zegrar F, Sahnoun M, Baltache H, Reshak A. (2006). Ab initio study of structural, electronic, elastic and high pressure properties of barium chalcogenides. *Computational Materials*

- Science 38263-270.  
<https://doi.org/10.1016/j.commat.2006.03.001>
- [46] REUSS A, Angew Z. (1929). Berechnung der fließgrenze von mischkristallen, berechnung der fließgrenze von mischkristallen auf grund der plastizitätsbedingung für einkristalle. MATH. MECH. 9: 55.  
<https://doi.org/10.1002/zamm.19290090104>
- [47] Cao Y, Zhu J, Liu Y, Lai Z, Nong Z. (2013). First-principles studies of the structural, elastic, electronic and thermal properties of  $\gamma'$ -Ni<sub>3</sub>Ti. Physica B: Condensed Matter 412: 45-49.  
<https://doi.org/10.1016/j.physb.2012.12.020>